HHS Public Access

Author manuscript

Eur J Neurosci. Author manuscript; available in PMC 2020 September 01.

Published in final edited form as:

Eur J Neurosci. 2019 September ; 50(5): 2801–2813. doi:10.1111/ejn.14429.

Ultrastructural localization of DREADDs in monkeys

Adriana Galvan[1,2], **Jessica Raper**[1], **Xing Hu**[1], **Jean-François Paré**[1], **Jordi Bonaventura**[3], **Christopher T. Richie**[4], **Michael Michaelides**[3,5], **Sascha A. L. Mueller**[6,7], **Patrick H. Roseboom**[6], **Jonathan A. Oler**[6], **Ned H. Kalin**[6,7,8], **Randy A. Hall**[9], **Yoland Smith**[1,2]

[1.] Yerkes National Primate Research Center, Emory University, Atlanta, GA, 30329, USA

[2.] Department of Neurology, Emory University School of Medicine, Atlanta GA, 30322 USA

[3.] Biobehavioral Imaging and Molecular Neuropsychopharmacology Unit, National Institute on Drug Abuse (NIDA), Intramural Research Program, National Institutes of Health, Baltimore, MD, 21224, USA

[4.] Genetic Engineering and Viral Vector Core, National Institute on Drug Abuse (NIDA), Intramural Research Program, National Institutes of Health, Baltimore, MD 21224, USA.

[5.] Department of Psychiatry, Johns Hopkins School of Medicine, Baltimore, MD 21205, USA

[6.] Department of Psychiatry, University of Wisconsin, Madison, WI

[7.] Molecular and Cellular Pharmacology Training Program, University of Wisconsin, Madison, WI

[8.] Wisconsin National Primate Research Center, Madison WI

[9.] Department of Pharmacology, Emory University School of Medicine, Atlanta, GA, USA, 30322

Abstract

Designer-receptors exclusively activated by designer drugs (DREADDs) are extensively used to modulate neuronal activity in rodents, but their use in primates remains limited. An essential need that remains is the demonstration that DREADDs are efficiently expressed on the plasma membrane of primate neurons. To address this issue, electron microscopy immunogold was used to determine the subcellular localization of the AAV vector-induced DREADDs hM4Di and hM3Dq fused to different tags in various brain areas of rhesus monkeys and mice. When hM4Di was fused to mCherry, the immunogold labeling was mostly confined to the intracellular space, and poorly expressed at the plasma membrane in monkey dendrites. In contrast, the hM4Di-mCherry labeling was mostly localized to the dendritic plasma membrane in mouse neurons, suggesting species differences in the plasma membrane expression of these exogenous proteins.

Corresponding author: Adriana Galvan, PhD, Yerkes National Primate Research Center, 954 Gatewood Road NE, Atlanta GA 30329, Phone: 404 712 8841, agalvan@emory.edu.

Author contributions

AG, JR, JB, MM, NK and YS designed the experiments. JR, XH, JFP, SM, PHR and JO collected the data. AG and XH analyzed the data. CTR made DNA plasmids. AG, JR, JB, MM, SM, PHR, JO, NK, RAH and YS interpreted the data. AG, JR, JB, SM, PHR, JO, NK, RAH and YS wrote the manuscript.

Conflict of interest

The authors report no conflict of interests

Data accessibility

Data are available upon request to the corresponding author.

The lack of hM4Di plasma membrane expression may limit the functional effects of systemic administration of DREADD-actuators in monkey neurons. Removing the mCherry and fusing of hM4Di with the hemagglutinin (HA) tag resulted in strong neuronal plasma membrane immunogold labeling in both monkeys and mice neurons. Finally, hM3Dq-mCherry was expressed mostly at the plasma membrane in monkey neurons, indicating that the fusion of mCherry with hM3Dq does not hamper membrane incorporation of this specific DREADD. Our results suggest that the pattern of ultrastructural expression of DREADDs in monkey neurons depends on the DREADD/tag combination. Therefore, a preliminary characterization of plasma membrane expression of specific DREADD/tag combinations is recommended when using chemogenetic approaches in primates.

Graphical Abstract

We examined the ultrastructural localization of the DREADDs hM4Di and hM3Dq fused to different tags in monkey and mouse neurons. Poor plasma membrane expression was observed with hM4Di-mCherry in monkeys. In contrast, strong plasma membrane localization was found with HA-hM4Di in mice and monkeys, hM4Di-mCherry in mice and hM3Dq-mCherry in monkeys. Our results suggest that ultrastructural expression of DREADDs depends on the species, and the DREADD/tag combination.

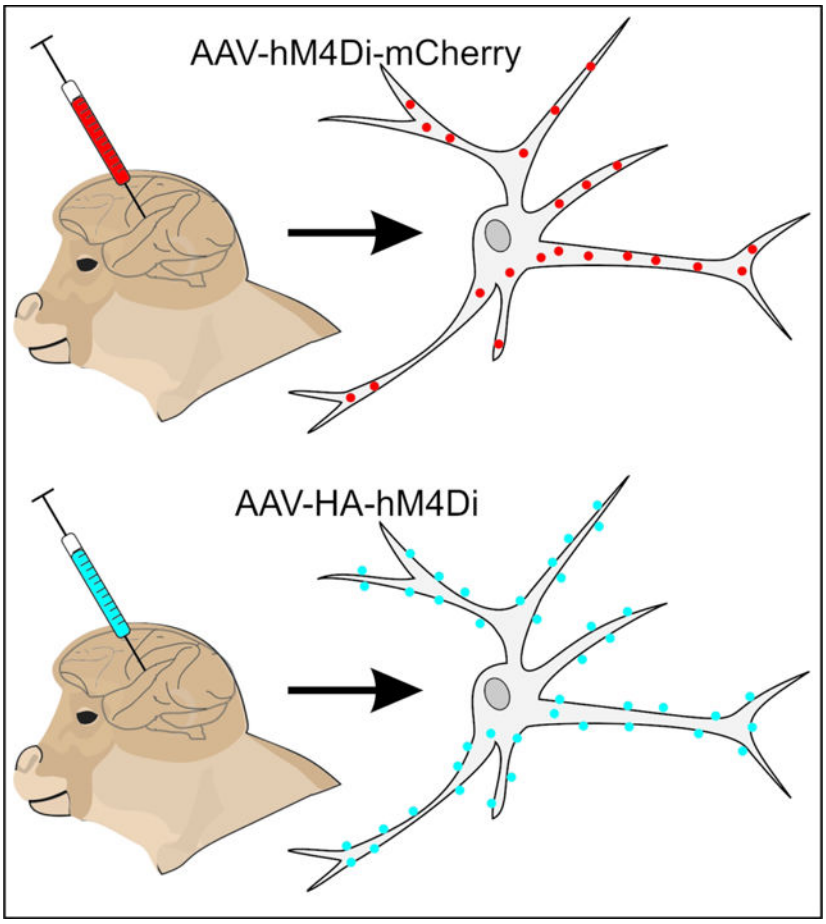

Keywords

immunogold; hM4Di; hM3Dq; mCherry; HA-tag

Introduction

Chemogenetic techniques based on Designer Receptors Exclusively Activated by Designer Drugs (DREADDs) have been extensively used to study brain circuits related to sleep, feeding, anxiety, and movement, among many others (Roth, 2016). Due to its minimal invasiveness, adjustability and reversibility, the chemogenetic approach is attractive to basic and translational neuroscience research, as it allows precise modulation of selected neuronal subpopulations, through systemic injections of pharmacological compounds that activate the DREADDs (Rogan & Roth, 2011; Sternson & Roth, 2014). The DREADD-based methods, however, have been applied mostly in rodent studies, while only a handful of reports using DREADDs in non-human primates (NHPs) have been published (Eldridge *et al.,* 2016; Grayson *et al.,* 2016; Nagai *et al.,* 2016; Upright *et al.,* 2018).

Because of the translational significance of NHP studies, based on the close evolutionary relationship between NHPs and humans (Capitanio & Emborg, 2008; Phillips *et al.,* 2014; Roelfsema & Treue, 2014), it is essential to optimize the use of DREADDs (and other chemogenetic approaches) for NHP studies, so as to confirm and expand the impressive advances already achieved in rodent models, and to take a step closer to using these promising techniques as therapeutic approaches for humans.

To further enable the effective use of DREADDs in NHPs and its potential utility for human interventions, it is important to characterize DREADDs expression at cellular and subcellular levels in NHPs. In published studies in which DREADDs have been used in NHPs, the receptor expression has been confirmed post-mortem by light-microscopy visualization of the tag proteins fused to the DREADDs (Eldridge *et al.,* 2016; Grayson *et al.,* 2016; Nagai *et al.,* 2016; Upright *et al.,* 2018). To help interpret the functional capacity of DREADDs, it is also important to demonstrate that DREADDs are inserted into the plasma membrane, where the receptors are functionally linked to their intracellular signaling pathways and can engage with their exogenous ligands (clozapine-n-oxide or clozapine, Armbruster *et al.,* 2007; Gomez *et al.,* 2017). High-resolution electron microscopic (EM) methods can be used to study the ultrastructural localization of endogenous or transduced receptors, including the spatial relationship of receptors and the cytoplasmic plasma membrane. In particular, the use of non-diffusible colloidal gold particles as markers of antigens in the EM-immunogold technique permits reliable localization of membrane proteins with nanometer resolution (Galvan *et al.,* 2006). Previously, we successfully used this approach in monkey tissue to demonstrate that the viral vector-induced expression of channelrhodopsins (ChR2) occurs primarily in the plasma membrane of striatal and thalamic neurons, where they can be effectively activated by light stimulation (Galvan *et al.,* 2012).

In the current study, we use the immunogold method to demonstrate that DREADDs can also be expressed in primate neuronal plasma membranes. The findings suggest that the specificity of the combination of the DREADD and the tag protein plays an important role in

the ability of the DREADD to be inserted in the plasma membrane in monkey neurons. The results of this work will help to refine strategies aimed at achieving the effective use of DREADDs in NHPs.

Methods

Animals

These studies were done in accordance with federal guidelines (NRC, 2011), and the United States Public Health Service Policy on the Humane Care and Use of Laboratory Animals (revised 2015), and were approved by the Animal Care and Use Committees at Emory University, University of Wisconsin-Madison and the National Institute on Drug Abuse (NIDA).

Five rhesus macaques (*Macaca mulatto,* 3 females and 2 males, ages 4 to 14 years old at the time of virus solution injection) were obtained from the colonies at the Yerkes National Primate Research Center (YNPRC, Atlanta, GA), or the Wisconsin National Primate Research Center (WNPRC, Madison, WI). The animals were housed in pairs (YNPRC), or single housed (WNPRC, due to a previous unrelated immunization study), maintained in a controlled environment with a 12-hour light/dark cycle, had free access to water, and were fed twice daily. Five mice (male, C57/Bl6J, 25–30g at the time of the injection) were ordered from Jackson Laboratory, and housed 4 per cage until surgery, and individually housed afterwards. They were fed regular chow and water *ad libitum* and maintained at a 12-hour light/dark cycle.

Viral vectors and intracerebral injections

Animals received adeno-associated virus encoding hM4Di or hM3Dq fused to mCherry at the C-terminus (AAV-hSyn-hM4Di-mCherry and AAV-hSyn-hM3Dq-mCherry plasmids provided by Dr. Bryan Roth, UNC) or hM4Di fused to HA tag at the N-terminus (AAV-hSyn-HA-hM4Di). To construct the AAV-hSyn-HA-hM4Di plasmid (Addgene plasmid # 121538 ; http://n2t.net/addgene:121538; RRID:Addgene_121538), the sequence encoding HA-tagged hM4D(Gi) was amplified from pAAV-hSyn-HA-hM4D(Gi)-IRES-mCitrine and used to replace the FLAG-tagged iRFP coding region in pOTTC1479 (pAAV SYN1 iRFP-FLAG, unpublished) using ligation-independent cloning. pAAV-hSyn-HA-hM4D(Gi)-IRES-mCitrine was a gift from Bryan Roth (Addgene plasmid # 50464; http://n2t.net/addgene:50464; RRID:Addgene_50464). Table 1 describes sources for the viral vectors, details of the injection sites, and volume of virus solution injected in each animal.

In monkey MR264, the injection of the virus solution followed procedures similar to those described in previous studies of amygdala lesions in monkeys (Raper *et al.,* 2014). Briefly, the monkey was sedated with ketamine hydrochloride (1mg/kg) and maintained with isoflurane (1–2% intratracheal) throughout the T1 weighted MRI scan to determine the stereotaxic coordinates of the amygdala. Under aseptic conditions and isoflurane anesthesia (1–2% to effect), craniotomies were made over the left and right amygdala and the viral vector solution was administered in six to eight injection sites within the center of the basolateral amygdala, using a 10 μl Hamilton syringe. Needles were lowered simultaneously

in both hemispheres, and the solution was infused at a rate of 0.4 μl/min. After each injection, a 3 min waiting period was allotted to minimize viral spread during needle retractions. Post-surgical treatments included banamine (1 mg/kg for 3 days), dexamethasone (0.5 mg/kg for 3 days), and rocephin, 25 mg/kg for 7 days) to prevent pain, edema, and infection, respectively.

In monkeys MR263 and MR275, the injections of the virus solution were done through chronically implanted recording chambers directed at the subthalamic nucleus (STN). The placement of chambers was done during a surgical procedure performed under anesthesia (1– 3% intratracheal isoflurane) and using aseptic techniques, as previously described (Galvan *et al.,* 2014). Post-surgical treatments were the same as those described above for monkey MR264. The injections of virus solutions were done under electrophysiological guidance, using a custom-made injection system combined with a tungsten electrode (Kliem & Wichmann, 2004). The injection-recording probes were lowered in the STN and the solution was infused at a rate of 0.1–0.2 μl /min, followed by a 10 min wait time before withdrawing the injection system.

In monkeys MR290 and MR293, targeting of the injection site and subsequent viral vector delivery were performed using intraoperative MRI (iMRI) methods (for details, see Kalin *et al.,* 2016). Briefly, before the procedure, the animals were anesthetized with ketamine (up to 20 mg/kg), prepared for surgery, and then placed in a magnetic resonance imaging (MRI)-compatible stereotaxic frame. The animals were intubated and received isoflurane anesthesia (1–3%, intratracheal). Injections of the viral vector solutions were done into the arcuate sulcus of the frontal cortex and the dorsal amygdala of the right hemisphere (MR290), or into cortical area 25 of the left hemisphere (MR293). The viral vector solution was infused along with 0.66 mM Gadobenate dimeglumine to visualize dispersion of the infusate on the MRI. After the surgery, cefazolin (20–25 mg/kg, twice daily for 5 days) and buprenorphine (up to 0.03 mg/kg, twice daily for one day) were given to prevent infection and minimize discomfort.

All monkey surgeries conducted at the YNPRC or WNPRC were done while monitoring vital signs, (heart rate, respiration, oxygen saturation, and CO_2), and post-surgical treatments were administered in coordination with the respective veterinary staff.

For intracerebral injections in mice, the animals were anesthetized with a mixture of ketamine (60 mg/kg) and xylazine (12 mg/kg), placed on a stereotaxic apparatus, and received bilateral injections of virus solution (Table 1) in the basolateral amygdala (BLA). Coordinates of injections to target the BLA were: 1.3 mm posterior, ±2.8 mm lateral and 5.0 mm ventral from Bregma (according to the Paxinos mouse brain atlas, (Paxinos & Franklin, 2012). Virus solutions were injected using a 2 μl Hamilton syringe over 10 min, at a rate of 50 nl/min, and the syringe was left in place for an additional 10 minutes to allow diffusion of the suspension. During surgery, mice body temperature was monitored and controlled using a heat pad during surgical procedures and recovery from anesthesia. After surgery, the animals were treated with a saline injection (20 ml/kg) for hydration, and carprofen (5 mg/kg) for analgesia.

Systemic injections of clozapine-n-oxide or clozapine

In the context of other studies that examined functional effects of DREADDs (not reported here), some of the monkeys received systemic injections of clozapine-n-oxide (10 mg/kg each time), while some of the mice and two monkeys received one injection of a trace dose of clozapine. Table 1 provides details of the number of injections done in each animal.

Perfusion and initial preparation of tissue

The animals received an overdose of pentobarbital, and were transcardially perfused with Ringer's solution, followed by 4% paraformaldehyde and 0.1% glutaraldehyde in phosphate buffer (T, 0.2 M, pH 7.4). After removing the brain from the skull, we collected vibratome coronal sections (60 μm) in cold phosphate-buffered saline (PBS, 0.01M, pH 7.4), that were stored at −20° C in an anti-freeze solution (30% ethylene glycol/30% glycerol in PB), until further processing (Table 1). The period of storage time in the freezer did not affect the quality of immunoreactivity.

Immunohistochemistry and processing of tissue for light and electron microscope

We used antibodies against mCherry or HA-tag and the pre-embedding immunogold method to examine the subcellular localization of hM4Di or hM3Dq. We first used light microscopy immunoperoxidase to localize the viral vector injection sites, and identify regions appropriate for the ultrastructural analysis. For this, we selected brain sections containing or adjacent to the virus solution injection tracks. Sections were pretreated with 1% normal goat serum, 1% bovine serum albumin and 0.3% Triton X-100, and then incubated in the respective antibody solution (mCherry or HA-Tag, Table 2) for 24 hours. This was followed by incubation in secondary biotinylated antibodies, then in Avidin-biotin-peroxidase complex (ABC) solution (1:200; Vectastain standard kit, Vector) for 90 min. The sections were then placed in 0.025% 3–3'-diaminobenzidine tetrahydrochloride (DAB, Sigma-Aldrich, St. Louis, MO), 0.01M Imidazole (Fisher Scientific, Pittsburgh, PA) and 0.006% H_2O_2 for 10 min. The sections were mounted on slides, cover-slipped, and digitized with an Aperio Scanscope CS system (Aperio Technologies, Vista, CA).

To conduct the ultrastructural analysis of the localization of DREADDs, we selected sections adjacent to those showing strong immunoperoxidase labeling. These sections were treated with 1% sodium borohydride (20 min), placed in a cryoprotectant solution (PB, 0.05 M, pH 7.4, containing 25% sucrose /10% glycerol) for 20 min, frozen at −80° C for 20 min, thawed and washed in PBS. Then, to block non-specific sites, the sections were immersed in PBS containing 5% non-fat dry milk (20 min), and subsequently washed three times in Tris-buffered saline (TBS)-gelatin (Tris 0.02 M, NaCl 0.15 M and 0.1% cold water fish gelatin, 10 min each wash). Control sections were incubated without the primary antibodies. The sections were incubated with the primary antibodies against mCherry or HA-Tag (Table 2) for 24 h. This was followed by rinses in TBS-gelatin and incubation in gold-conjugated secondary antibodies (Table 2) for 2 h. Primary and secondary antibodies were diluted in TBS-gelatin buffer containing 1% dry milk, and antibody incubations were done at room temperature.

The sections were then washed with TBS-gelatin and 2% acetate buffer (pH 7.0) and the gold labeling was silver-intensified (HQ silver; Nanoprobes) for 9–13 min in the dark. The intensification process was stopped by washing several times with acetate buffer. The tissue was then post-fixed in osmium tetroxide (0.5% in 0.1 M PB, pH 7.4), rinsed in PB, and dehydrated by incubating the sections sequentially in 50%, 70% (plus uranyl acetate 1%), 90% and 100% ethanol (10–15 min in each solution, 100% ethanol incubation was repeated twice). Then, the sections were incubated in propylene oxide for 10 min. After post-fixation, the sections were embedded in resin (Durcupan ACM; Fluka, Ft. Washington, PA) on microscope slides, and placed in a 60°C oven for 48 h to polymerize the resin. The sections were examined under the light microscope, and blocks of tissue in the regions of interest were cut and glued onto resin blocks. Ultrathin (60 nm) sections were obtained with an ultramicrotome (Ultracut T2; Leica, Nussloch, Germany) and collected on pioloform-coated copper grids. Sections were stained with lead citrate for 5 min to increase their contrast during EM visualization. The sections were examined with an electron microscope (JEOL model 1011, Peabody, MA) at 20,000–25,000X, and areas containing immunogold particles were photographed with a digital camera (DualView 300W; Gatan, Inc., Pleasanton, CA) controlled by Digital Micrograph software (Gatan).

Analysis of material

Only micrographs obtained from areas with optimal ultrastructural preservation of brain tissue were used for the analysis. We collected a minimum of 25 immunogold-labeled elements (dendrites or terminals) per case. The number of elements collected varied per case depending on the areas of tissue with optimal ultrastructural preservation. The localization and quantification of labeling in the micrographs were assessed using ImageJ (Rasband, 1997; Schneider *et al.,* 2012). Structures containing gold particles were categorized into dendrites or axonal terminals, based on ultrastructural features (Peters *et al.,* 1991). Silver enhancement confers variable sizes to immunogold particles, which sometimes results in particle accumulations or clusters, in which individual gold particles are not easily defined. To quantify gold particles in clusters, discernable circular contours in the cluster were counted as individual particles. In cases where the cluster was amorphous, it was counted as one particle.

For the analysis, only dendrites or axon terminals of which the full length of the plasma membrane was clearly visible in the micrograph were selected. Based on the size of primary and secondary antibodies (~17 nm, Blackstad *et al.,* 1990) plus the radius of the gold particle (0.7 nm), a particle was categorized as “plasma membrane bound” if it was located within ~18 nm from the membrane (measurements were done using ImageJ). All other gold particles were categorized as “intracellular”. The proportion of plasma membrane-bound or intracellular particles was expressed as a fraction of the total number of gold particles within specific neuronal elements (dendrite or terminal). To analyze the relationship between the proportion of plasma membrane-bound gold particles and species (monkey or mouse), tag protein (mCherry or HA) or DREADD type (hM4Di or hM3Dq), we used a linear mixed effects model (SPSS version 24, IBM), that defined species, tag protein and DREADD type as fixed factors, and individual virus injections as random factor.

Finally, we examined the localization of plasma-membrane bound gold particles in relation to synapses, in the cases where synaptic densities were observed. Plasma membrane-bound gold particles were classified into extrasynaptic, if they were attached to parts of the plasma membrane not involved in synapses; or synaptic, if they were located in the main body of postsynaptic specializations. Synapses were classified as symmetric or asymmetric, or remained not classified when a clear identification was not possible.

Results

Localization of injection sites, selection of regions of interest and overall quantification

To identify the areas with strong DREADDs transduction, we used antibodies against mCherry or HA-tag, and revealed these antibodies using biotinylated antibodies and immunoperoxidase. Figure 1 shows representative images of brain sections close to the viral vector injection sites in some of the animals used in this study. In these sections, the core of the injection sites and the related spread of labeling could be assessed by the diffusion of the amorphous brown immunoperoxidase staining generated by DAB staining. Sections adjacent to those depicted in this figure were used for the ultrastructural analyses of DREADD localization in the electron microscope, using immunogold methods. Table 3 describes the total number or elements (dendrites or terminals) sampled and gold particles counted in each case.

Ultrastructural localization of hM4Di-mCherry

Three monkeys received injections of AAV-hSyn-hM4Di-mCherry (one of them in BLA, and the other two animals in the STN). Representative low-magnification images of the injection sites are shown in Fig. 1A and 1B.

The ultrastructural location of hM4Di-mCherry was analyzed at the EM level using immunogold. The majority of immunogold particles (85% of total number of particles, average for the four injections), were found in the intracellular space. The cellular organelles to which the gold particles were attached were putatively identified as microtubules or agranular reticulum. Only a small proportion of gold particles were localized on the plasma membrane (Fig. 2A-C, see summary of data in Fig. 5). This pattern of localization of hM4Di-mCherry was similar in the three monkeys, regardless of the injected target nuclei (basolateral amygdala or the subthalamic nucleus) or the AAV serotype (AAV5 or AAV8).

To investigate if this pattern of hM4Di-mCherry subcellular expression was specific to the monkey brain tissue, two mice were injected with AAV-hSyn-hM4Di-mCherry in BLA (Fig. 1C). The expression of hM4Di-mCherry in mice was strikingly different from that observed in monkeys. A large proportion of hM4Di-mCherry in mouse tissue was bound to the plasma membrane (64% of all particles, average for the 2 mice, Fig. 5), while a smaller fraction was observed in the intracellular compartment (Fig. 2D-E). These results suggest that the hM4Di-mCherry fusion has limited access to the dendritic plasma membrane of neurons in monkeys, but not in mice.

Ultrastructural localization of HA-hM4Di

Given the limited expression of hM4Di-mCherry at the plasma membrane in monkey neurons, we hypothesized that the use of a different tag fused to the hM4Di might improve the transport of this DREADD to the plasma membrane. The hemagglutinin (HA) tag is an epitope of the hemagglutinin of the influenza virus. Since its introduction thirty years ago (Field *et al.,* 1988), the HA-tag has been extensively used to label proteins. Thus, we tested if the use of HA-tag fused to hM4Di could improve the transport of this receptor to the plasma membrane.

One monkey received two injections of AAV-hSyn-HA-hM4Di, one in the amygdala (Fig. 1E) and the second in the arcuate sulcus of the frontal cortex (not shown, light microscopy pattern of expression was similar to that observed in the amygdala). We conducted an ultrastructural analysis using immunogold particles to reveal antibodies against HA-tag. In striking contrast to the results obtained with hM4Di-mCherry, we found that the majority of HA-hM4Di immunogold labeling was bound to the plasma membrane in the monkey brain tissue (Fig. 3A-C). Only 7% of gold particles were localized in the intracellular space (Fig. 5). Similarly, in mice that received AAV-hSyn-HA-hM4Di in the amygdala (Fig. 1D), 94% of gold particles on average were bound to the plasma membrane (Fig. 3D-F, and Fig. 5). These results indicate that the fusion of HA-tag greatly improves the trafficking of hM4Di to the membrane, relative to fusion with mCherry. A linear mixed effects model confirmed that species, tag protein and the interaction of species and tag protein, were significant predictors of plasma membrane-bound particles (species: $F_{(1, 7.1)}=116.3$, $p<0.0001$; tag protein: $F_{(1, 7.1)}=567.4$, $p<0.0001$; interaction of species and tag protein: $F_{(1, 7.1)}=112.6$, $p<0.001$).

Ultrastructural localization of hM3Dq-mCherry

To investigate if the limited transport to the plasma membrane of hM4Di-mCherry was a general feature of mCherry-fused DREADDs in monkeys, we studied the ultrastructural localization of hM3Dq-mCherry, after viral injections were performed in area 25 of cortex of one monkey (Fig. 1F). In contrast to what we observed with the hM4Di-mCherry, we found that 83% of gold particles labeling hM3Dq-mCherry were bound to the plasma membrane (Fig. 4, and Fig. 5). In agreement, a linear mixed effect model showed that, when the DREADD is fused to mCherry, the type of DREADD can predict the proportion of plasma membrane-bound particles in monkey neurons ($F_{(1, 2.2)}=291.6$, $p=0.002$). This observation suggests that fusion to mCherry does not hamper the transport of all DREADDS to the dendritic plasma membrane in monkey neurons, and that specific DREADD/Tag combinations exhibit different neuronal plasma membrane expression patterns.

Finally, we examined if plasma membrane-bound particles revealing hM4Di-mCherry, HA-Tag or hM3Dq-mCherry were associated with synapses. In all cases, and for both species, the immunogold particles were very rarely found at synapses; with only 0.1 to 1.4% of total plasma membrane-bound particles located at the main body of synaptic specializations. However, as we and others have previously reported, the pre-embedding immungold method may lead to false negative synaptic labeling for plasma-membrane bound receptors, perhaps due to the antibodies being hindered from accessing the antigenic sites in the synaptic cleft (Baude *et al.,* 1993; Nusser *et al.,* 1994; Galvan *et al.,* 2006).

Discussion

Using the immunogold method and electron microscopic analysis, we have described the ultrastructural localization of hM4Di and hM3Dq in monkeys and mice.

We found that, in monkeys, hM4Di is poorly transported to the plasma membrane when fused to the mCherry tag protein. Conversely, a large proportion of immunogold particles revealing hM4Di-mCherry were observed at the plasma membrane in mouse neurons. The different expression patterns of hM4Di-mCherry between monkeys and mice suggests an important species difference in the intracellular trafficking and/or membrane insertion of these foreign proteins, although it is unclear why this is the case.

The pattern of hM4Di-mCherry expression in mice, with most of the gold-particles bound to the plasma membrane, is consistent with the robust behavioral effects observed during hM4Di-mediated neuronal silencing in numerous rodent studies (reviewed in Sternson & Roth, 2014; Roth, 2016). On the other hand, our findings suggest that the effects of systemically applied DREADD-activating compounds may be compromised by the low proportion of hM4Di at the plasma membrane in monkey neurons. However, it is possible that when activated by the exogenous compound, only a small number of plasma-membrane hM4Di receptors are necessary to decrease neuronal firing. Indeed, two studies have reported functional effects of hM4Di-mCherry activation in monkeys. In one study, hM4Di-mCherry receptors were expressed in the amygdala, and CNO injections altered amygdalo-cortical functional connectivity (Grayson *et al.,* 2016), while in the second study CNO-mediated activation of hM4Di-mCherry in prefrontal cortex disrupted spatial working memory (Upright *et al.,* 2018). Other studies, using a lentiviral vector to express hM4Di fused to cyan fluorescent protein (Eldridge *et al.,* 2016) or hM4Di without a tag protein (Nagai *et al.,* 2016) also showed behavioral changes with hM4Di activation in monkeys. Overall, these positive results strongly support use of DREADDs to modulate neuronal activity in monkeys. Furthermore, we suggest that increased trafficking of the receptors to the plasma membrane has the potential to facilitate more robust and consistent effects of chemogenetic silencing in monkeys.

The monkeys that were injected with AAV5-hSyn-hM4Di-mCherry received several systemic injections of CNO, while the mice were not treated with this drug (Table 2). Receptor internalization is known to occur for G-protein coupled receptors after agonist exposure (Gainetdinov *et al.,* 2004), so we cannot completely rule out the possibility that the large proportion of hM4Di-mCherry gold particles found in the intracellular compartment in monkey neurons was a result of internalization. However, this is unlikely, because in our study there was an interval of at least 15 days (and up to 143 days; see Table 1) between the last CNO injection and euthanasia, allowing washing out of the drug and restoration of receptors to basal conditions (Brancaccio *et al.,* 2013; Anaclet *et al.,* 2015).

In contrast to the findings with hM4Di-mCherry, the same receptor showed robust plasma membrane expression when fused to the HA-tag, in both monkey and mouse neurons. Compared to mCherry, which is 256 amino acids, the HA tag is a small 9 amino acid fragment of hemagglutinin (Field *et al.,* 1988). Given its small size, the fact that it can be

readily detected using antibodies (Green *et al.,* 1982), and the fact that it does not appear to interfere with the function of most recombinant proteins, this tag has been extensively used as a general epitope tag in viral vectors. Our results suggest that the HA tag is advantageous over mCherry when fused to hM4Di, because it does not hamper the positioning of hM4Di in the plasma membrane in primate neurons. The HA-tag is fused to the hM4Di at the N-terminus, leaving the C-terminus unhindered to incorporate with scaffolding proteins that might anchor the receptor to the membrane (Ritter & Hall, 2009).

One potential confound of our study is that the monkeys that received AAV-hM4Di-mCherry and those that received AAV-HA-hM4Di were obtained from different colonies, and the injections were done using slightly different methods. However, the improved trafficking of the hM4Di to the plasma membrane in the presence of the HA-tag was also observed in mice, further supporting the notion that this construct does not interfere with membrane trafficking of DREADDs. Our results suggest that hM4Di fused to HA could be a better and more reliable tool than hM4Di-mCherry to be used in monkey DREADD-related experiments. An additional consideration that favors HA over mCherry is that the expression of fluorescent proteins can induce immune responses and neuroinflammation in NHPs (Samaranch *et al.,* 2014).

We also studied the localization of hM3Dq-mCherry in monkey neurons, and found that the fusion of this excitatory DREADD with the mCherry protein did not prevent transport to the plasma membrane. It is possible that structural differences between hM4Di and hM3Dq could account for the discrepant patterns of localization when fused to mCherry. For instance, the C-terminus is shorter in the M4 receptor than in the M3 receptor (Kruse *et al.,* 2014). It is possible that a large tag protein (such as mCherry) fused to the C-terminus may be spaced far enough away from the receptor's transmembrane core and cytoplasmic loops so it does not interfere with efficient membrane incorporation. In contrast, fusion of the same tag to the M4 receptor's shorter C-terminus may interfere with the transmembrane core and either globally perturb receptor folding or hinder interactions with chaperone proteins that are necessary for proper plasma membrane transport, anchoring and/or recycling. Thus, the inclusion of mCherry fused to a DREADD does not always result in poor plasma membrane incorporation in primate neurons, but rather, the fusion of mCherry to specific exogenous proteins (i. e., hM4Di) can interfere with expression at the plasma membrane. Consistent with this idea, fusion of mCherry with the opsin ChR2 results in a lower expression level of the opsin than were observed upon ChR2 fusion to yellow fluorescent protein (Yazdan-Shahmorad *et al.,* 2018).

A limitation of our study is that the observations of hM3Dq-mCherry localization were based on a single injection in one monkey. However, these data provide the first description of the ultrastructural localization of hM3Dq (in monkeys or other species), and suggests that the fusion of mCherry to hM3Dq does not hamper the incorporation of the receptor to the membrane, supporting the use of this construct in DREADD-related studies in monkeys.

In summary, this study reveals that the choice of tags to visualize the expression of DREADDs can significantly affect their subcellular localization and, presumably, their function in the primate brain. In addition, our observations suggest that the expression

patterns of some exogenous proteins may not be the same in primate and rodent neurons, therefore highlighting the need to understand potential species-specific differences in viral vector-transduced protein expression. This consideration is of utmost importance in non-human primate experiments, where the number of subjects is typically low and the possibility of repeated experiments is limited. Thus, strategies to optimize the expression of DREADDs in NHPs, such as careful selection of tags to identify the receptor, can help further advance both the research and therapeutic use of chemogenetic approaches in monkeys and humans.

Acknowledgements

We thank Susan Jenkins for technical assistance, the staffs of the Yerkes National Primate Research Center (YNPRC), the Harlow Center for Biological Psychology, the HealthEmotions Research Institute at the University of Wisconsin-Madison, and the Wisconsin National Primate Research Center (WNPRC). We also thank Drs. Mark Baxter, Michael Caiola and Thomas Wichmann for constructive comments. We acknowledge the UNC Gene Therapy Vector Core and Dr. R. Jude Samulski, Addgene, and Boston Children's Hospital Viral Core for manufacturing viral vectors used in this study. This work was funded by National Institutes of Health Office of Research Infrastructure Programs OD P51-OD011132 to the YNPRC, P51-OD011106 to the WNPRC, grant R01-MH046729 to NHK and National Institute on Drug Abuse Intramural Research Program support DA00069 to MM.

Abbreviations

AAV	adeno-associated virus
BLA	basolateral amygdala
ChR2	channelrhodopsin
CLZ	clozapine
CNO	clozapine-N-oxide
d	dendrite
DREADDs	designer-receptors exclusively activated by designer drugs
EM	electron microscope
HA	hemagglutinin
NHP	non-human primate
PB	phosphate buffer
PBS	phosphate-buffered saline
STN	subthalamic nucleus
t	axon terminal
TBS	tris-buffered saline

References

Anaclet C, Pedersen NP, Ferrari LL, Venner A, Bass CE, Arrigoni E & Fuller PM (2015) Basal forebrain control of wakefulness and cortical rhythms. Nat Commun, 6, 8744. [PubMed: 26524973]

Armbruster BN, Li X, Pausch MH, Herlitze S & Roth BL (2007) Evolving the lock to fit the key to create a family of G protein-coupled receptors potently activated by an inert ligand. Proc Natl Acad Sci U S A, 104, 5163–5168. [PubMed: 17360345]

Baude A, Nusser Z, Roberts JD, Mulvihill E, McIlhinney RA & Somogyi P (1993) The metabotropic glutamate receptor (mGluR1 alpha) is concentrated at perisynaptic membrane of neuronal subpopulations as detected by immunogold reaction. Neuron, 11, 771–787. [PubMed: 8104433]

Blackstad TW, Karagulle T & Ottersen OP (1990) MORFOREL, a computer program for two-dimensional analysis of micrographs of biological specimens, with emphasis on immunogold preparations. Comput Biol Med, 20, 15–34. [PubMed: 2328575]

Brancaccio M, Maywood ES, Chesham JE, Loudon AS & Hastings MH (2013) A Gq-Ca2+ axis controls circuit-level encoding of circadian time in the suprachiasmatic nucleus. Neuron, 78, 714–728. [PubMed: 23623697]

Capitanio JP & Emborg ME (2008) Contributions of non-human primates to neuroscience research. Lancet, 371, 1126–1135. [PubMed: 18374844]

Eldridge MA, Lerchner W, Saunders RC, Kaneko H, Krausz KW, Gonzalez FJ, Ji B, Higuchi M, Minamimoto T & Richmond BJ (2016) Chemogenetic disconnection of monkey orbitofrontal and rhinal cortex reversibly disrupts reward value. Nat Neurosci, 19, 37–39. [PubMed: 26656645]

Field J, Nikawa J, Broek D, MacDonald B, Rodgers L, Wilson IA, Lerner RA & Wigler M (1988) Purification of a RAS-responsive adenylyl cyclase complex from Saccharomyces cerevisiae by use of an epitope addition method. Mol Cell Biol, 8, 2159–2165. [PubMed: 2455217]

Gainetdinov RR, Premont RT, Bohn LM, Lefkowitz RJ & Caron MG (2004) Desensitization of G protein-coupled receptors and neuronal functions. Annu Rev Neurosci, 27, 107–144. [PubMed: 15217328]

Galvan A, Hu X, Rommelfanger KS, Pare JF, Khan ZU, Smith Y & Wichmann T (2014) Localization and function of dopamine receptors in the subthalamic nucleus of normal and parkinsonian monkeys. J Neurophysiol, 112, 467–479. [PubMed: 24760789]

Galvan A, Hu X, Smith Y & Wichmann T (2012) In vivo optogenetic control of striatal and thalamic neurons in non-human primates. PLoS One, 7, e50808.

Galvan A, Kuwajima M & Smith Y (2006) Glutamate and GABA receptors and transporters in the basal ganglia: what does their subsynaptic localization reveal about their function? Neuroscience, 143, 351–375. [PubMed: 17059868]

Gomez JL, Bonaventura J, Lesniak W, Mathews WB, Sysa-Shah P, Rodriguez LA, Ellis RJ, Richie CT, Harvey BK, Dannals RF, Pomper MG, Bonci A & Michaelides M (2017) Chemogenetics revealed: DREADD occupancy and activation via converted clozapine. Science, 357, 503–507. [PubMed: 28774929]

Grayson DS, Bliss-Moreau E, Machado CJ, Bennett J, Shen K, Grant KA, Fair DA & Amaral DG (2016) The Rhesus Monkey Connectome Predicts Disrupted Functional Networks Resulting from Pharmacogenetic Inactivation of the Amygdala. Neuron, 91, 453–466. [PubMed: 27477019]

Green N, Alexander H, Olson A, Alexander S, Shinnick TM, Sutcliffe JG & Lerner RA (1982) Immunogenic structure of the influenza virus hemagglutinin. Cell, 28, 477–487. [PubMed: 6176330]

Kalin NH, Fox AS, Kovner R, Riedel MK, Fekete EM, Roseboom PH, Tromp do PM, Grabow BP, Olsen ME, Brodsky EK, McFarlin DR, Alexander AL, Emborg ME, Block WF, Fudge JL & Oler JA (2016) Overexpressing Corticotropin-Releasing Factor in the Primate Amygdala Increases Anxious Temperament and Alters Its Neural Circuit. Biol Psychiatry, 80, 345–355. [PubMed: 27016385]

Kliem MA & Wichmann T (2004) A method to record changes in local neuronal discharge in response to infusion of small drug quantities in awake monkeys. J Neurosci Methods, 138, 45–49. [PubMed: 15325110]

Kruse AC, Kobilka BK, Gautam D, Sexton PM, Christopoulos A & Wess J (2014) Muscarinic acetylcholine receptors: novel opportunities for drug development. Nat Rev Drug Discov, 13, 549–560. [PubMed: 24903776]

Nagai Y, Kikuchi E, Lerchner W, Inoue KI, Ji B, Eldridge MA, Kaneko H, Kimura Y, Oh-Nishi A, Hori Y, Kato Y, Hirabayashi T, Fujimoto A, Kumata K, Zhang MR, Aoki I, Suhara T, Higuchi M, Takada M, Richmond BJ & Minamimoto T (2016) PET imaging-guided chemogenetic silencing reveals a critical role of primate rostromedial caudate in reward evaluation. Nat Commun, 7, 13605. [PubMed: 27922009]

NRC (2011) Guide for the Care and Use of Laboratory Animals: Eighth Edition. The National Academies Press, Washington, DC.

Nusser Z, Mulvihill E, Streit P & Somogyi P (1994) Subsynaptic segregation of metabotropic and ionotropic glutamate receptors as revealed by immunogold localization. Neuroscience, 61, 421–427. [PubMed: 7969918]

Paxinos G & Franklin KBJ (2012) The Mouse Brain in Stereotaxic Coordinates. Academic Press, Sidney, Australia.

Peters A, Palay S & Webster HD (1991) The Fine Structure of the Nervous System. Oxford University Press, New York.

Phillips KA, Bales KL, Capitanio JP, Conley A, Czoty PW, t Hart BA, Hopkins WD, Hu SL, Miller LA, Nader MA, Nathanielsz PW, Rogers J, Shively CA & Voytko ML (2014) Why primate models matter. Am J Primatol, 76, 801–827. [PubMed: 24723482]

Raper J, Stephens SB, Henry A, Villarreal T, Bachevalier J, Wallen K & Sanchez MM (2014) Neonatal amygdala lesions lead to increased activity of brain CRF systems and hypothalamic-pituitary-adrenal axis of juvenile rhesus monkeys. J Neurosci, 34, 11452–11460. [PubMed: 25143624]

Rasband W (1997) ImageJ US National Institutes of Health, Bethesda, MD.

Ritter SL & Hall RA (2009) Fine-tuning of GPCR activity by receptor-interacting proteins. Nat Rev Mol Cell Biol, 10, 819–830. [PubMed: 19935667]

Roelfsema PR & Treue S (2014) Basic neuroscience research with nonhuman primates: a small but indispensable component of biomedical research. Neuron, 82, 1200–1204. [PubMed: 24945764]

Rogan SC & Roth BL (2011) Remote control of neuronal signaling. Pharmacol Rev, 63, 291–315. [PubMed: 21415127]

Roth Bryan L. (2016) DREADDs for Neuroscientists. Neuron, 89, 683–694. [PubMed: 26889809]

Samaranch L, San Sebastian W, Kells AP, Salegio EA, Heller G, Bringas JR, Pivirotto P, DeArmond S, Forsayeth J & Bankiewicz KS (2014) AAV9-mediated expression of a non-self protein in nonhuman primate central nervous system triggers widespread neuroinflammation driven by antigen-presenting cell transduction. Mol Ther, 22, 329–337. [PubMed: 24419081]

Schneider CA, Rasband WS & Eliceiri KW (2012) NIH Image to ImageJ: 25 years of image analysis. Nat Meth, 9, 671–675.

Sternson SM & Roth BL (2014) Chemogenetic tools to interrogate brain functions. Annu Rev Neurosci, 37, 387–407. [PubMed: 25002280]

Upright NA, Brookshire SW, Schnebelen W, Damatac CG, Hof PR, Browning PGF, Croxson PL, Rudebeck PH & Baxter MG (2018) Behavioral effect of chemogenetic inhibition is directly related to receptor transduction levels in rhesus monkeys. J Neurosci.

Yazdan-Shahmorad A, Tian N, Kharazia V, Samaranch L, Kells A, Bringas J, He J, Bankiewicz K & Sabes PN (2018) Widespread optogenetic expression in macaque cortex obtained with MR-guided, convection enhanced delivery (CED) of AAV vector to the thalamus. J Neurosci Methods, 293, 347–358. [PubMed: 29042259]

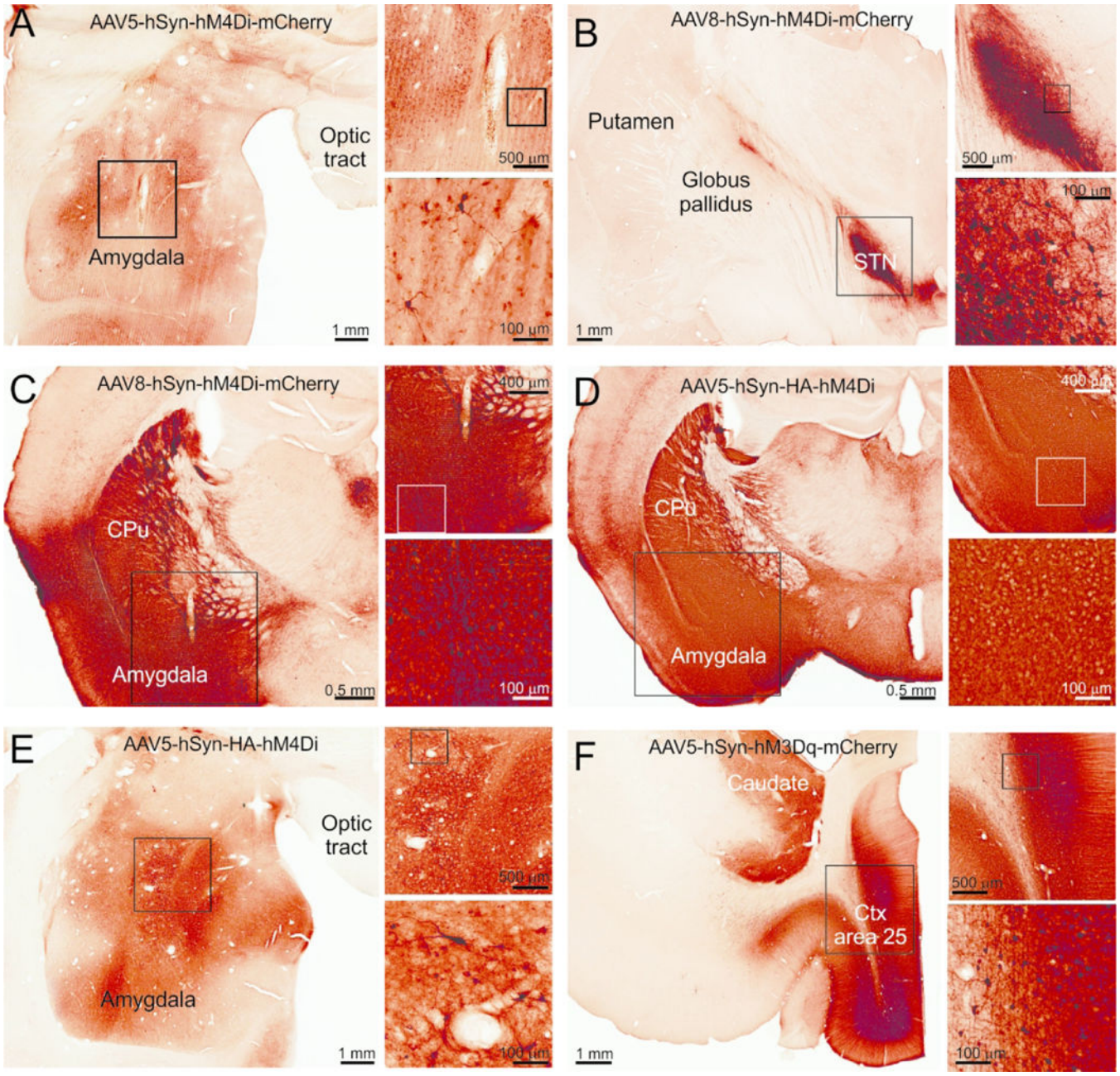

Figure. 1: Representative images showing expression of DREADDs in monkey and mouse brain tissue after viral vector injections.

The immunoperoxidase method was used to reveal the tag proteins fused to the DREADDs. All the sections are adjacent or at the site of the injection track. A) Monkey MR264, B) Monkey MR275, C) Mouse RM9, D) Mouse RM34, E) Monkey MR290, F) Monkey MR293. In each panel, the rectangles indicate areas that are shown at higher magnification in the subsequent images.

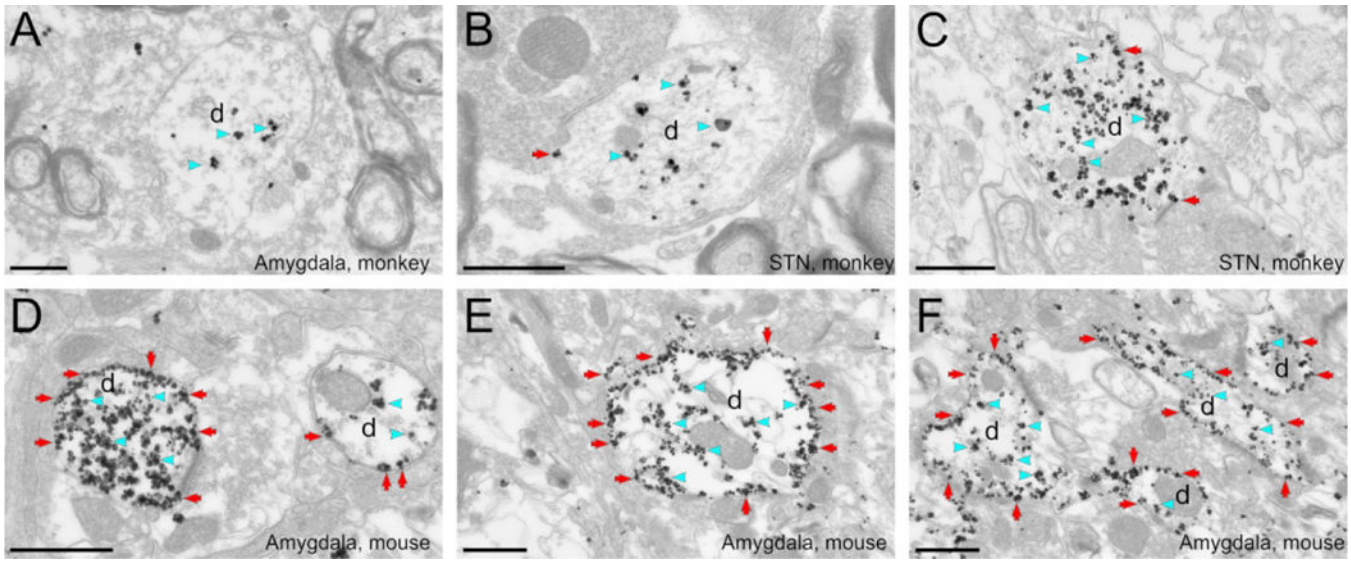

Figure 2. Ultrastructural localization of hM4Di-mCherry in monkeys and mice.

The pre-embedding immunogold method was used to reveal the hM4Di-mCherry. **A to C:** Electron micrographs showing examples of labeled dendrites in monkey amygdala (A) or STN (B, C). Immunogold particles labeling for hM4Di-mCherry is found mostly in the intracellular compartment (blue arrowheads). **D to F:** Electron micrographs of labeled dendrites in mice amygdala. The bulk of hM4Di-mCherry gold particles labeling is bound to the plasma membrane (red arrows). All scale bars= 0.6 μm. d, dendrite.

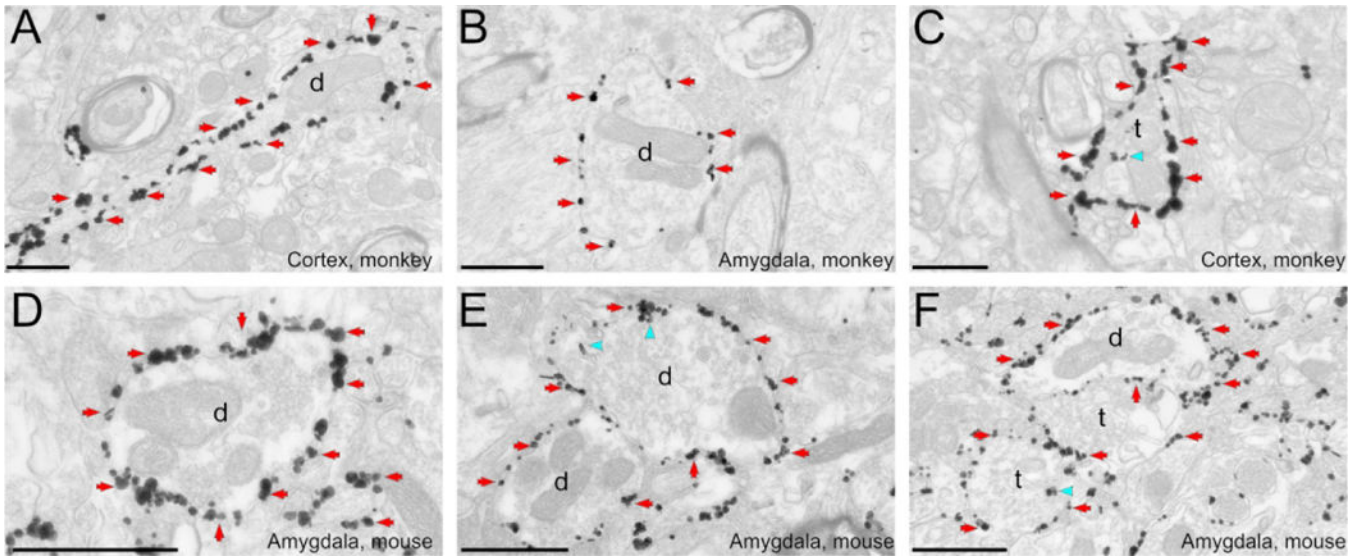

Figure 3: HA-hM4Di localization in monkeys and mice.

The immunogold method was used to reveal HA-hM4Di. **A to C:** Electron micrographs of labeled dendrites in the monkey arcuate sulcus (A,C) or amygdala (B). **D to F:** Electron micrographs of immunoreactive dendrites in the mouse amygdala. Most gold particles indicating HA-hM4Di are bound to the plasma membrane in both monkey and mice tissue. Blue arrowheads and red arrows point to examples of intracellular and plasma membrane-bound gold particles, respectively. All scale bars= 0.6 μm. d, dendrite; t, axon terminal

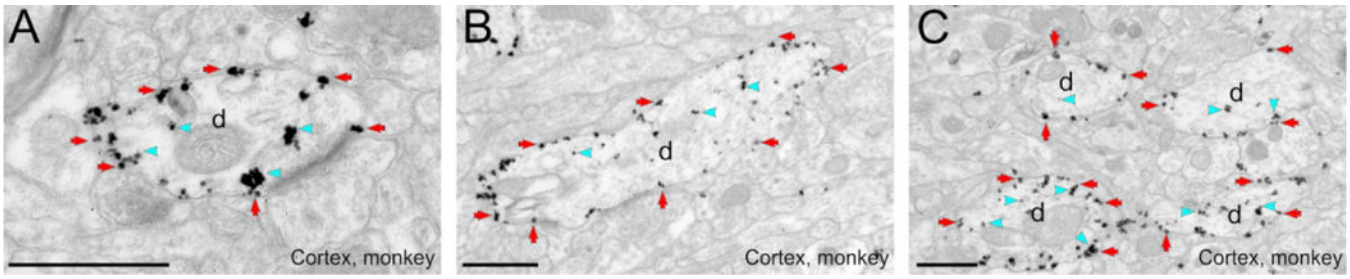

Figure 4: hM3Dq-mCherry localization in monkey, as revealed with immunogold.

Electron micrographs of labeled dendrites in the monkey cortex, area 25. hM3Dq dendritic labeling is mostly bound to the plasma membrane. Blue arrowheads and red arrows point to examples of intracellular and plasma membrane bound gold particles, respectively. All scale bars= 0.6 μm. d, dendrite

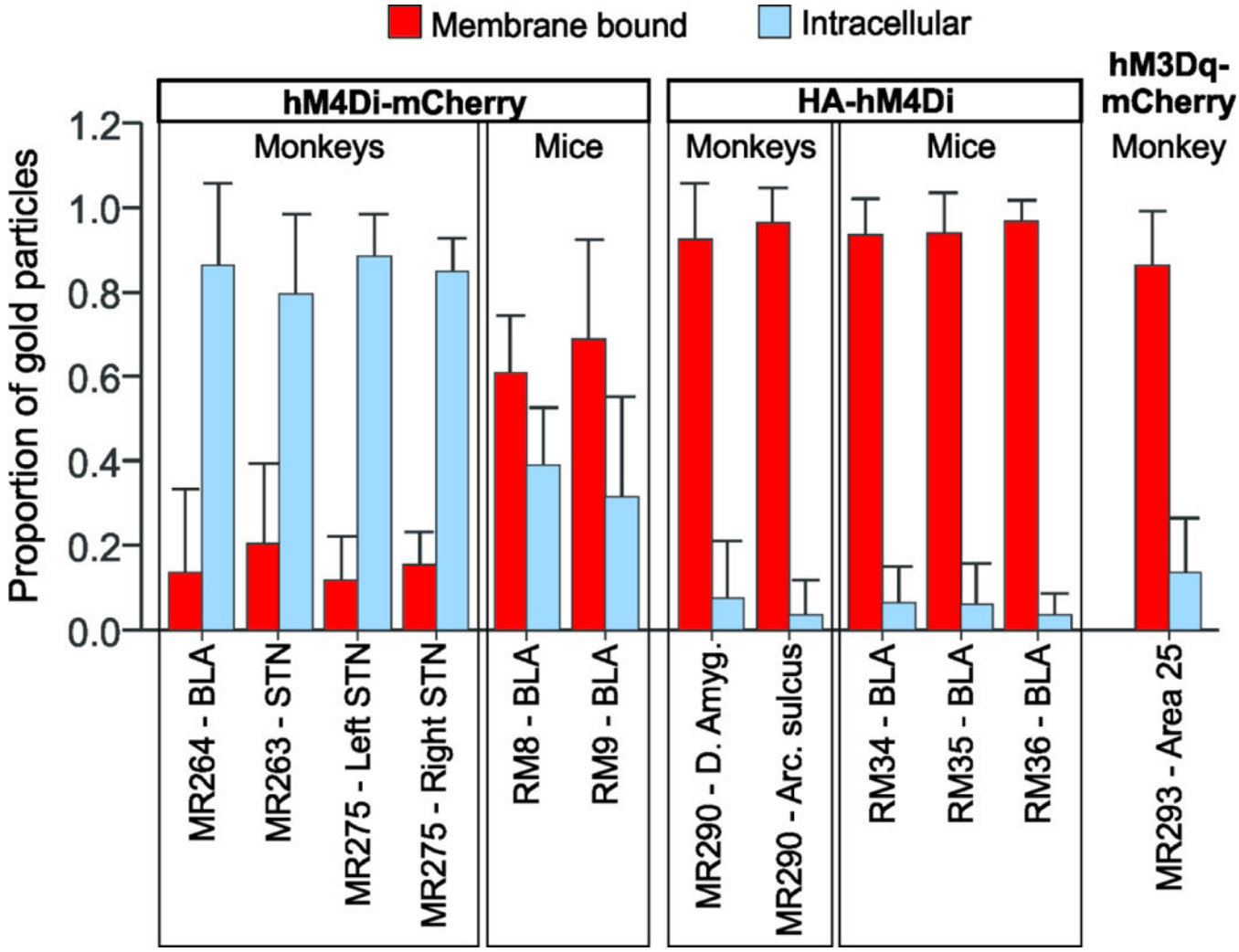

Figure 5: Summary of ultrastructural localization of DREADDs, as revealed by immunogold localization

Proportion of gold particles bound to the plasma membrane (red) and in the intracellular compartment (blue) of labeled elements. Data are means + SD (the number of elements quantified for each case is shown in Table 3).

Table 1:

Details of viral injections and systemic injections

Animal ID	Species	Injection location	Vector	Titer (vg/ml)	Amount injected, (µl)	Number of systemic CNO or CLZ injections	Survival days after viral injection	Survival days after last CNO or CLZ injection	Days from perfusion to immunohisto-chemistry
MR264	Rhesus macaque	BLA, left[#]	AAV5-hSyn-hM4Di-mCherry[a]	1.3×10^{13}	40	9	651	73	180
MR263	Rhesus macaque	STN, left	AAV5-hSyn-hM4Di-mCherry[a]	4.1×10^{13}	10	3	70	15	181
MR275	Rhesus macaque	STN, left	AAV5-hSyn-hM4Di-mCherry[a]	4.1×10^{13}	12	27	417	143	62
		STN, right	AAV8-hSyn-hM4Di-mCherry[a]	2×10^{12}	28		279		
MR290	Rhesus macaque	Dorsal amygdala, right	AAV5-hSyn-HA-hM4Di[c]	6.9×10^{13}	24	1[*]	36	7	139
		Frontal cortex, right			15				50
MR293	Rhesus macaque	Cortex area 25	hSyn-hM3Dq-mCherry[a]	3.4×10^{12}	22	1[*]	41	14	96
RM8, RM9	Mice	BLA, bilateral	AAV8-hSyn-hM4Di-mCherry[b]	3×10^{12}	1	0	9	n/a	42
RM34, RM35, RM36	Mice	BLA,bilateral	AAV5-hSyn-HA-hM4Di[c]	4.25×10^{12}	0.3 (per side)	1[*]	35	7	36

Viral vector sources:

[a]University of North Carolina Vector Core,

[b]Addgene,

[c]Boston Children's Hospital Viral Core

Abbreviations: CNO, clozapine-N-oxide; CLZ, clozapine

[#]For monkey MR264, only the injection in the left BLA was examined, due to poor tissue preservation in the right hemisphere.

[*]Only one injection of trace dose of [C11]-clozapine

Table 2:

Sources and concentrations of antibodies

Antibody	Vendor	Catalog number	Antibody registry number	Host	Concentration used
Anti-mCherry	Abcam, Cambridge, MA	AB167453	AB_2571870	Rabbit	1:1,000
Anti-HA Tag (clone C29F4)	Cell Signaling Technology, Danvers, MA	3724	AB_1549585	Rabbit	1:400
Gold-conjugated anti-rabbit, (1. 4 nm gold particle size)	Nanoprobes, Stony Brook, NY	2004	AB_2631182	Goat	1:100
Biotinylated anti-rabbit	Vector Laboratories, Burlingame, CA	BA-1000	AB_2313606	Goat	1:200

Table 3:

Number of elements and particles quantified for each injection site

Animal ID	Species	Injection location	Vector	No. elements counted	Intra-cymiddlelasmic particles	Membrane-bound particles
MR264	Rhesus macaque	BLA, center	AAV5-hSyn-hM4Di-mCherry[a]	25	429	63
MR263	Rhesus macaque	STN, left	AAV5-hSyn-hM4Di-mCherry[a]	93	1291	271
MR275	Rhesus macaque	STN, left	AAV5-hSyn-hM4Di-mCherry[a]	26	752	106
		STN, right	AAV8-hSyn-hM4Di-mCherry[a]	33	2587	489
MR290	Rhesus macaque	Dorsal amygdala, right	AAV5-hSyn-HA-hM4Di[c]	83	102	947
		Frontal cortex, right		48	62	1564
MR293	Rhesus macaque	Cortex area 25	hSyn-hM3Dq-mCherry[a]	150	838	4130
RM8	Mouse	BLA, bilateral	AAV8-hSyn-hM4Di-mCherry[b]	52	1260	1772
RM9	Mouse	BLA, bilateral	AAV8-hSyn-hM4Di-mCherry[b]	39	388	866
RM34	Mouse	BLA, bilateral	AAV5-hSyn-HA-hM4Di[c]	32	92	1299
RM35	Mouse	BLA, bilateral	AAV5-hSyn-HA-hM4Di[c]	55	134	1903
RM36	Mouse	BLA, bilateral	AAV5-hSyn-HA-hM4Di[c]	38	68	1566